ELSEVIER

Engineering Analysis with Boundary Elements 26 (2002) 355–366

ENGINEERING ANALYSIS *with* BOUNDARY ELEMENTS

www.elsevier.com/locate/enganabound

Efficient evaluation of three-dimensional Green's functions in anisotropic elastostatic multilayered composites

B. Yang*, E. Pan

Structures Technology, Inc., 543 Keisler Drive, Ste 204, Cary, NC 17511, USA

Received 7 January 2001; revised 26 October 2001; accepted 21 November 2001

Abstract

The three-dimensional Green's functions in anisotropic elastostatic multilayered composites (MLCs) obtained within the framework of generalized Stroh formalism are expressed as two-dimensional integrals of Fourier inverse transform over an infinite plane. Their numerical evaluations involve tremendous computational efforts in particular in the presence of various singularities and near-singularities due to the presence of material mismatches across interfaces. The present paper derives the complete set of the Green's functions including displacement, stress and their derivatives with respect to source coordinates using a novel and computationally efficient approach. It is proposed for the first time that the Green's functions in the MLCs are expressed as a sum of a special solution and a general-part solution, with the former consisting of the first few terms of the trimaterial expansion solution around a source load. Since the zero-order term contains the singularity corresponding to the homogeneous full-space solution and can be evaluated analytically, and the other higher-order terms contain most of the near-singular behaviors and can be reduced to a line integral over a finite interval, the general-part solution becomes regular and the Green's functions overall can be evaluated efficiently. As an example, the Green's functions in a five-layered orthortropic plate are evaluated to demonstrate the efficiency of the proposed approach. Also, the detailed characteristics of these Green's functions are examined in both the transform- and physical-domains. These Green's functions are essential in developing the boundary-integral-equation formulation and numerical boundary element method for composite laminate problems involving regular and cracked geometries.

Keywords: 3D Green's functions; Anisotropic elasticity; Multilayered structures; Stroh formalism; Fourier transforms

1. Introduction

Green's functions are essential to the boundary integral equation (BIE) formulation for various engineering problems. They can also be used to solve various inclusion problems with the eigenstrain in the inclusion being regarded as an equivalent body-force source [1]. While various two-dimensional (2D) and three-dimensional (3D) Green's functions in isotropic elasticity and 2D Green's functions in anisotropic elasticity have been derived so far, relatively slow progress has been made for the corresponding 3D Green's functions in anisotropic elasticity [2]. During recent years, however, the generalized Stroh formalism has been used to derive certain Green's functions in 3D anisotropic elasticity (see, for example, Refs. [2–4]), originated from the classical work of Barnett and Lothe [5]. Since the Green's functions are first solved in the 2D Fourier transform domain, one major challenge is to invert analytically the Fourier inverse transform to obtain the physical-domain Green's functions. For a 3D anisotropic elastostatic full-space, Ting and Lee [6], Sales and Gray [7], and Tonon et al. [8] derived the Green's functions in an explicit form. While Wu [3] derived the anisotropic half-space Green's functions as a line integral over a finite interval, Pan and Yuan [4] derived the corresponding bimaterial Green's functions. More recently, Yang and Pan [9] derived the 3D Green's functions for anisotropic trimaterials using an expansion approach. In the expansion approach, each term in the series can be expressed as a line integral over a finite interval, similar to the bimaterial solution [4].

The Green's functions in multilayered composites (MLCs) hold special interests in various engineering branches [10–14]. For 3D composite laminates and layered half space of anisotropic elasticity, Yuan and Yang [15] presented a boundary value (B.V.) problem formulation for the Green's displacement and stress within the generalized Stroh formalism by imposing the interfacial continuity conditions and the appropriate boundary conditions, similar to the parallel works for MLCs of isotropic and transversely

* Corresponding author. Tel.: +1-919-816-0434; fax: +1-919-816-0438.
E-mail address: bobyang@ustc.edu (B. Yang).

0955-7997/02/$ - see front matter
PII: S0955-7997(02)00002-4

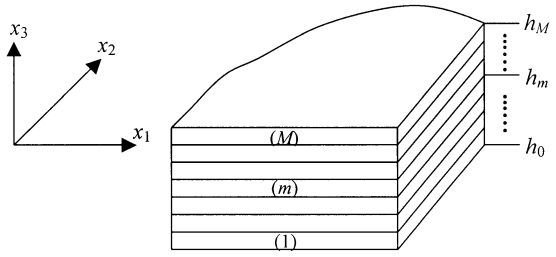

Fig. 1. An M-layered composite with perfectly bonded interfaces. A Cartesian coordinate system (x_1,x_2,x_3) is attached to the composite plate.

isotropic elasticity [13]. Their solutions are expressed in two parts: a special solution consisting of the homogeneous full-space solution and a general-part solution, and were implemented into a 3D BIE formulation for the stress analysis around holes in composite laminates [16]. However, since the general-part solution involves inevitably a numerical 2D integration in an infinite plane and a solution of a large system of algebraic equations at each mesh point for the inverse transform, the special solution consisting of only the homogeneous full-space solution results in an inefficient evaluation of the Green's functions. This is particularly true when the source and field points both are close to or on the same interface. In the present work, we therefore propose a novel approach of evaluation of the Green's functions in MLCs by incorporating the trimaterial expansion solutions recently developed by the authors [9]. It is shown that this new approach improves significantly the efficiency on evaluation of the Green's functions. With the derivatives of the Green's displacement and stress with respect to source coordinates also being derived in this paper, a BIE formulation based on these Green's functions can then be developed in application to various problems of anisotropic MLCs with regular and cracked geometries [17].

This paper is organized as follows. In Section 2, a B.V. problem for anisotropic elastostatic MLCs is formulated under the conditions of free traction on one surface and rigid-smooth contact (i.e. frictionless contact on a rigid plane) on the other, along with perfectly bonded interfaces. While the generalized Stroh formalism is applied to solve the B.V. problem, the Green's displacement, stress and their derivatives are developed in the Fourier transform domain. In Section 3, a novel approach for the numerical evaluation (Fourier inverse transform) of the MLCs Green's functions is proposed for the first time in which the special solution consists of the first few terms in the trimaterial expansion solution developed recently by Yang and Pan [9]. In Section 4, the proposed evaluation approach of the Green's functions is implemented numerically. Through an example of a five-layered orthortropic plate, it is found that the incorporation of the zero- and first-order terms into the special solution produces the most efficient numerical evaluation for the Green's functions in the material. Furthermore, the detailed characteristics of these Green's functions in both the transform- and physical-domains are examined. Finally, some conclusions are drawn in Section 5.

2. Green's functions in anisotropic elastostatic MLCs

2.1. Problem formulation

Consider a laterally infinite composite plate made of M different layers each of uniform thickness, as shown in Fig. 1. A Cartesian coordinate system (x_1,x_2,x_3) is attached to the plate, with the x_3-axis perpendicular to the surfaces. The materials within each layer are homogeneous, anisotropic and linearly elastic, and the interfaces between the layers are perfectly bonded. The Hooke's law for each material layer is given by

$$\boldsymbol{\sigma}_{ij} = \mathbf{C}_{ijkl}\boldsymbol{\varepsilon}_{kl}, \tag{1}$$

where $\boldsymbol{\sigma}_{ij}$ is the stress tensor, $\boldsymbol{\varepsilon}_{kl}$ the strain tensor related to the displacement vector $\mathbf{u}_i$ by $\boldsymbol{\varepsilon}_{kl} = (u_{k,l} + u_{l,k})/2$, and $\mathbf{C}_{ijkl}$ the elastic stiffness tensor consisting of 21 independent elements in general and different for the layers. Note that the standard notation system is used in the text. All Latin subscript indices range from 1 to 3. Greek subscript indices range from 1 to 2. A bold symbol for a tensor implies its subscript indices in the range from 1 to 3. Summation over repeated subscripts over their range is implied.

Assume that a point-force $\mathbf{f}$ is applied to the composite plate at a source point $\mathbf{X}$, the equilibrium equation at a field point $\mathbf{x}$ can be written, in the absence of other body forces, as

$$\sigma_{ij,j}(\mathbf{x}) = -f_i\delta(\mathbf{x} - \mathbf{X}) \tag{2}$$

and thus, by substituting the constitutive law,

$$C_{ijkl}(\mathbf{x})u_{k,lj}(\mathbf{x}) = -f_i\delta(\mathbf{x} - \mathbf{X}) \tag{3}$$

where $\delta(\mathbf{x} - \mathbf{X})$ is the Dirac delta function, and the subscript $,lj$ indicates the partial derivatives with respect to x_l and x_j sequentially. Eq. (3) is valid for each homogeneous layer with the elastic stiffness tensor C_{ijkl} being substituted accordingly.

The perfectly bonded condition along interfaces is given by

$$\begin{aligned} &\mathbf{u}_m = \mathbf{u}_{m+1}, \\ &\mathbf{t}_m = \mathbf{t}_{m+1}, \ \text{ at } x_3 = h_m, \ \text{for } m = 1,\ldots,M-1, \end{aligned} \tag{4}$$

where $\mathbf{t} = \sigma\mathbf{n}$ with $\mathbf{n} = (0,0,1)^{\mathrm{T}}$ in which T denotes transpose of a vector or matrix, and h_m is the vertical level of the interface between the mth and $(m+1)$th layers (Fig. 1).

Various boundary conditions may be applied to the bottom and top surfaces of the plate. However, not all of them produce physically admissible solutions, as discussed on the Green's functions for 3D plate problems under a number of boundary conditions by Yang and Pan [18]. In the present paper, the traction-free condition on the bottom

surface and the rigid-smooth contact condition on the top surface are considered, as expressed, respectively, by

$$\mathbf{t} = 0, \quad \text{at } x_3 = h_0, \tag{5}$$

$$t_1 = t_2 = u_3 = 0, \quad \text{at } x_3 = h_M, \tag{6}$$

where h_0 and h_M are the vertical levels of the bottom and top surfaces, respectively.

In addition, it is required that as $|\mathbf{x}|$ approaches infinity, the solution $\mathbf{u}$ vanishes, i.e.

$$\lim_{|x|\to\infty} \mathbf{u}(\mathbf{x}) = 0. \tag{7}$$

This is called the radiation condition for a point-source solution.

Eqs. (3)–(7) together form a well-posed B.V. problem in anisotropic elastostatics. Solutions to this B.V. problem are called Green's functions for the composite plate due to a point force. In order to derive the solution, the generalized Stroh formalism [2,4,5] is adopted, as described in Section 2.2.

2.2. Solutions by the generalized Stroh formalism

Within the generalized Stroh formalism, first the following 2D Fourier transform (y_1,y_2) is applied to the in-plane coordinates (x_1,x_2) of a field quantity, for instance, of u_i, as

$$\tilde{u}_i(y_1, y_2, x_3) = \int\int u_i(x_1, x_2, x_3) \mathrm{e}^{\mathrm{i}x_\alpha y_\alpha}\, \mathrm{d}x_1\, \mathrm{d}x_2, \tag{8}$$

where e stands for the exponential function, and i over e denotes the unit of imaginary number, $\sqrt{-1}$. The integral limits are $(-\infty, \infty)$ for both coordinates x_1 and x_2. Thus, in the Fourier transform domain, the governing Eq. (3) becomes

$$C_{i3k3}\tilde{u}_{k,33} - \mathrm{i}(C_{i\alpha k3} + C_{i3k\alpha})y_\alpha \tilde{u}_{k,3} - C_{i\alpha k\beta} y_\alpha y_\beta \tilde{u}_k = -f_i\, \mathrm{e}^{\mathrm{i}X_\alpha y_\alpha} \delta(x_3 - X_3). \tag{9}$$

Solving this ordinary differential equation in terms of x_3 with $\mathbf{f}$ being a unit force in the ith direction yields the general expression for the transform-domain Green's displacement in the jth direction, $\tilde{u}^*_{ji}$, as

$$\tilde{\mathbf{u}}^*_m(x_3) = \mathrm{e}^{\mathrm{i}y_\alpha X_\alpha}\Big[\tilde{\mathbf{u}}^{*(s)}_m(x_3) + \mathrm{i}\eta^{-1}(\bar{\mathbf{A}}_m\langle \mathrm{e}^{-\mathrm{i}\bar{\mathbf{p}}_m \eta(x_3 - h_{m-1})}\rangle \mathbf{V}_m + \mathbf{A}_m\langle \mathrm{e}^{-\mathrm{i}\mathbf{p}_m \eta(x_3 - h_m)}\rangle \mathbf{W}_m)\Big], \tag{10}$$

where the subscript m indicates the quantities associated to the mth layer where the field point $\mathbf{x}$ resides; $\tilde{\mathbf{u}}^*_m$ is a function of y_1,y_2 and $\mathbf{X}$ as well as x_3; $\tilde{\mathbf{u}}^{*(s)}_m$, a special solution, is a given function of y_1,y_2 and $\mathbf{X}$ as well as x_3; and $\mathbf{V}_m$ and $\mathbf{W}_m$ are a pair of unknown tensors, being functions of y_1, y_2 and X_3, to be determined by the boundary and interfacial conditions. The dummy arguments in these functions, which are not relevant directly to the following enforcement of boundary and interfacial conditions, are omitted for simplicity. In addition, the overbar denotes the complex conjugate, (η,θ) are the polar coordinates related to (y_1,y_2) by $y_1 = \eta\cos\theta$ and $y_2 = \eta\sin\theta$, $\mathbf{p}$ and $\mathbf{A}$ as functions of θ and C_{ijkl} are the eigenvalues and eigenvectors of the generalized Stroh eigenproblem [2], and

$$\langle \mathrm{e}^{-\mathrm{i}\mathbf{p}\eta x_3}\rangle \equiv \mathrm{diag}[\mathrm{e}^{-\mathrm{i}p_1\eta x_3}, \mathrm{e}^{-\mathrm{i}p_2\eta x_3}, \mathrm{e}^{-\mathrm{i}p_3\eta x_3}]. \tag{11}$$

Note that Eq. (10) satisfies the radiation condition (7) as long as the special solution, $\tilde{\mathbf{u}}^{*(s)}_m$, satisfies it. It is also noted that a superscript asterisk has been attached to the displacement to dictate that it is the fundamental solution. From the fundamental solution, the Green's function due to a point force in an arbitrary direction can be derived.

Let $\mathbf{s}$ be a vector containing the stress components in a plane parallel to the interface, namely, the in-plane stress vector. Combination of the out-of-plane traction solution $\mathbf{t}^* \equiv (\sigma^*_{13i}, \sigma^*_{23i}, \sigma^*_{33i})$ and the in-plane stress solution $\mathbf{s}^* \equiv (\sigma^*_{11i}, \sigma^*_{12i}, \sigma^*_{22i})$, with the subscript i being the point-force direction, then contains all the six independent stress components. By the constitutive law Eq. (1), $\mathbf{t}^*$ and $\mathbf{s}^*$ can be derived in the transform domain as

$$\tilde{\mathbf{t}}^*_m(x_3) = \mathrm{e}^{\mathrm{i}y_\alpha X_\alpha}\Big[\tilde{\mathbf{t}}^{*(s)}_m(x_3) + (\bar{\mathbf{B}}_m\langle \mathrm{e}^{-\mathrm{i}\bar{\mathbf{p}}_m \eta(x_3 - h_{m-1})}\rangle \mathbf{V}_m + \mathbf{B}_m\langle \mathrm{e}^{-\mathrm{i}\mathbf{p}_m \eta(x_3 - h_m)}\rangle \mathbf{W}_m)\Big], \tag{12}$$

$$\tilde{\mathbf{s}}^*_m(x_3) = \mathrm{e}^{\mathrm{i}y_\alpha X_\alpha}\Big[\tilde{\mathbf{s}}^{*(s)}_m(x_3) + (\bar{\mathbf{C}}_m\langle \mathrm{e}^{-\mathrm{i}\bar{\mathbf{p}}_m \eta(x_3 - h_{m-1})}\rangle \mathbf{V}_m + \mathbf{C}_m\langle \mathrm{e}^{-\mathrm{i}\mathbf{p}_m \eta(x_3 - h_m)}\rangle \mathbf{W}_m)\Big], \tag{13}$$

where $\tilde{\mathbf{t}}^{*(s)}_m$ and $\tilde{\mathbf{s}}^{*(s)}_m$ are assumed to be given as being derived from $\tilde{\mathbf{u}}^{*(s)}_m$, and the matrix $\mathbf{B}$ and $\mathbf{C}$ are related to $\mathbf{A}$ and $\mathbf{p}$, as functions of θ and C_{ijkl} [2,4]. Note that the matrix $\mathbf{C}$ here is different from the fourth-rank elastic stiffness tensor C_{ijkl}. For clarity, the elastic stiffness tensor always is written in its component form in this paper.

The derivatives of $\tilde{\mathbf{u}}^*$, $\tilde{\mathbf{t}}^*$ and $\tilde{\mathbf{s}}^*$ with respect to $\mathbf{X}$ can be obtained from the above expressions, as

$$\tilde{\mathbf{u}}^*_{m,X_\alpha}(x_3) = \mathrm{i}y_\alpha \tilde{\mathbf{u}}^*_m(x_3), \qquad \tilde{\mathbf{t}}^*_{m,X_\alpha}(x_3) = \mathrm{i}y_\alpha \tilde{\mathbf{t}}^*_m(x_3), \qquad \tilde{\mathbf{s}}^*_{m,X_\alpha}(x_3) = \mathrm{i}y_\alpha \tilde{\mathbf{s}}^*_m(x_3), \tag{14}$$

$$\tilde{\mathbf{u}}^*_{m,X_3}(x_3) = \mathrm{e}^{\mathrm{i}y_\alpha X_\alpha}\Big[\tilde{\mathbf{u}}^{*(s)}_{m,X_3}(x_3) + \mathrm{i}\eta^{-1}(\bar{\mathbf{A}}_m\langle \mathrm{e}^{-\mathrm{i}\bar{\mathbf{p}}_m \eta(x_3 - h_{m-1})}\rangle \mathbf{V}'_m + \mathbf{A}_m\langle \mathrm{e}^{-\mathrm{i}\mathbf{p}_m \eta(x_3 - h_m)}\rangle \mathbf{W}'_m)\Big], \tag{15}$$

$$\tilde{\mathbf{t}}^*_{m,X_3}(x_3) = \mathrm{e}^{\mathrm{i}y_\alpha X_\alpha}\Big[\tilde{\mathbf{t}}^{*(s)}_{m,X_3}(x_3) + (\bar{\mathbf{B}}_m\langle \mathrm{e}^{-\mathrm{i}\bar{\mathbf{p}}_m \eta(x_3 - h_{m-1})}\rangle \mathbf{V}'_m + \mathbf{B}_m\langle \mathrm{e}^{-\mathrm{i}\mathbf{p}_m \eta(x_3 - h_m)}\rangle \mathbf{W}'_m)\Big], \tag{16}$$

$$\tilde{\mathbf{s}}^{*}_{m,X_3}(x_3) = \mathrm{e}^{\mathrm{i}y_\alpha X_\alpha}\Big[\tilde{\mathbf{s}}^{*(s)}_{m,X_3}(x_3) + (\bar{\mathbf{C}}_m\langle \mathrm{e}^{-\mathrm{i}\bar{\mathbf{p}}_m\eta(x_3-h_{m-1})}\rangle\mathbf{V}'_m + \mathbf{C}_m\langle \mathrm{e}^{-\mathrm{i}\mathbf{p}_m\eta(x_3-h_m)}\rangle\mathbf{W}'_m)\Big], \tag{17}$$

where the subscript $,X_k$ denotes the partial differentiation with respect to source coordinate X_k, $\mathbf{V}'_m$ and $\mathbf{W}'_m$ are a new pair of unknown tensors, as functions of y_1, y_2 and X_3, to be determined by the boundary and interfacial conditions.

With the expressions of displacement and traction derived above, the boundary and interfacial conditions in Eqs. (4)–(6) can then be imposed (in the transform domain), resulting in a system of algebraic equations,

$$\tilde{\mathbf{t}}^{*(s)}_1(h_0) + (\bar{\mathbf{B}}_1\mathbf{V}_1 + \mathbf{B}_1\langle \mathrm{e}^{-\mathrm{i}\mathbf{p}_1\eta(h_0-h_1)}\rangle\mathbf{W}_1) = 0, \tag{18}$$

$$\begin{aligned}&\tilde{\mathbf{u}}^{*(s)}_m(h_m) + \mathrm{i}\eta^{-1}(\bar{\mathbf{A}}_m\langle \mathrm{e}^{-\mathrm{i}\bar{\mathbf{p}}_m\eta(h_m-h_{m-1})}\rangle\mathbf{V}_m + \mathbf{A}_m\mathbf{W}_m)\\ &\quad= \tilde{\mathbf{u}}^{*(s)}_{m+1}(h_m) + \mathrm{i}\eta^{-1}(\bar{\mathbf{A}}_{m+1}\mathbf{V}_{m+1}\\ &\qquad+ \mathbf{A}_{m+1}\langle \mathrm{e}^{-\mathrm{i}\mathbf{p}_{m+1}\eta(h_m-h_{m+1})}\rangle\mathbf{W}_{m+1}),\quad \text{for } m\\ &\quad= 1,\ldots,M-1,\end{aligned} \tag{19}$$

$$\begin{aligned}&\tilde{\mathbf{t}}^{*(s)}_m(h_m) + (\bar{\mathbf{B}}_m\langle \mathrm{e}^{-\mathrm{i}\bar{\mathbf{p}}_m\eta(h_m-h_{m-1})}\rangle_{\mathbf{V}m} + \mathbf{B}_m\mathbf{W}_m)\\ &\quad= \tilde{\mathbf{t}}^{*(s)}_{m+1}(h_m) + (\bar{\mathbf{B}}_{m+1}\mathbf{V}_{m+1}\\ &\qquad+ \mathbf{B}_{m+1}\langle \mathrm{e}^{-\mathrm{i}\mathbf{p}_{m+1}\eta(h_m-h_{m+1})}\rangle\mathbf{W}_{m+1}),\quad \text{for } m\\ &\quad= 1,\ldots,M-1,\end{aligned} \tag{20}$$

$$\tilde{\mathbf{g}}^{*(s)}_M(h_M) + (\bar{\mathbf{G}}_M\langle \mathrm{e}^{-\mathrm{i}\bar{\mathbf{p}}_M\eta(h_M-h_{M-1})}\rangle\mathbf{V}_M + \mathbf{G}_M\mathbf{W}_M) = 0. \tag{21}$$

In Eq. (21), $\tilde{\mathbf{g}}^{*}$ and $\mathbf{G}$ are defined in accordance with the symmetric (rigid-smooth contact) condition on the top surface, as

$$\begin{aligned}\tilde{\mathbf{g}}^{*} &\equiv \begin{pmatrix} t^{*}_{11} & t^{*}_{12} & t^{*}_{13}\\ t^{*}_{21} & t^{*}_{22} & t^{*}_{23}\\ u^{*}_{31} & u^{*}_{32} & u^{*}_{33}\end{pmatrix} \text{ and } \mathbf{G}\\ &\equiv \begin{pmatrix} B_{11} & B_{12} & B_{13}\\ B_{21} & B_{22} & B_{23}\\ \mathrm{i}\eta^{-1}A_{31} & \mathrm{i}\eta^{-1}A_{32} & \mathrm{i}\eta^{-1}A_{33}\end{pmatrix}.\end{aligned} \tag{22}$$

Eqs. (18)–(21) form a linear system of $2M$ algebraic equations with $2M$ unknowns of $\mathbf{V}_m$ and $\mathbf{W}_m$ ($m = 1,\ldots,M$). Therefore, $\mathbf{V}_m$ and $\mathbf{W}_m$ can be determined for each given set of y_1, y_2 and X_3 by solving this system of equations. Subsequently, the fundamental displacement, stress and their derivatives with respect to X_1 and X_2 are obtained in the transform domain.

Similarly, by inserting the expressions for the derivatives of these functions with respect to X_3 to the boundary and interfacial conditions (in the transform domain), a linear system of algebraic equations with the same number of unknowns can be formed. Again, the unknowns $\mathbf{V}'_m$ and $\mathbf{W}'_m$ can then be solved for each given set of y_1, y_2 and X_3, resulting in the solution to the derivatives of the fundamental displacement and stress with respect to X_3.

Once the transform-domain solutions are found, the corresponding physical-domain solutions can be derived by the Fourier inverse transform. For instance, the physical-domain displacement can be expressed as

$$u_i(x_1,x_2,x_3) = \frac{1}{(2\pi)^2}\int\int \tilde{u}_i(y_1,y_2,x_3)\mathrm{e}^{-\mathrm{i}x_\alpha y_\alpha}\,\mathrm{d}y_1\,\mathrm{d}y_2, \tag{23}$$

where the integral limits in both y_1 and y_2 are $(-\infty,\infty)$. The inverse transform may also be carried out in the polar coordinates (η,θ), instead of (y_1,y_2), as

$$u_i(x_1,x_2,x_3) = \frac{1}{(2\pi)^2}\int\int \eta\tilde{u}_i(\eta,\theta,x_3)\mathrm{e}^{-\mathrm{i}\eta(x_1\cos\theta + x_2\sin\theta)}\,\mathrm{d}\eta\,\mathrm{d}\theta, \tag{24}$$

where $0 < \eta < \infty$ and θ over the period of 2π. It is seen that, in terms of either integral expression, the integration needs in general to be evaluated numerically in the whole plane. Even with the Fast Fourier Transform (FFT) technique, the computational effort may become very large, prohibiting an efficient numerical implementation of the BIE formulation using these Green's functions. Therefore, it would be very appreciable if the involved 2D integrals can be reduced in dimensions analytically.

3. A novel approach for numerical evaluation of the Green's functions

In Section 2, the Green's functions in the MLCs are derived as a sum of two parts, namely, the special and general-part solutions. The special solution remains to be specified yet, and the general-part solution is expressed in terms of $\mathbf{V}_m$, $\mathbf{W}_m$, $\mathbf{V}'_m$ and $\mathbf{W}'_m$, which in turn are solved depending on the given special solution. Since no explicit expression generally is available for $\mathbf{V}_m$, $\mathbf{W}_m$, $\mathbf{V}'_m$ and $\mathbf{W}'_m$, the inverse of the general-part solution involves a numerical 2D integral over an infinite plane and a solution of a large system of equations at each mesh point. Therefore, it is desirable that the special solution includes terms whose Fourier inverse integral dimensions can be reduced analytically and also takes a large share of the total solution. In doing so, the computational effort in evaluating the remaining general-part solution can be reduced, leading to an appreciable reduction in the total computational time.

Based on the analysis of the transform-domain solutions, a novel approach is proposed to accurately and efficiently evaluate the physical-domain Green's functions in the MLCs. Specifically, the special solution incorporates the trimaterial expansion solution recently developed by Yang and Pan [9] as follows: If the field point $\mathbf{x}$ is located in a layer adjacent to or the same as the layer $m_{\mathbf{X}}$ where the

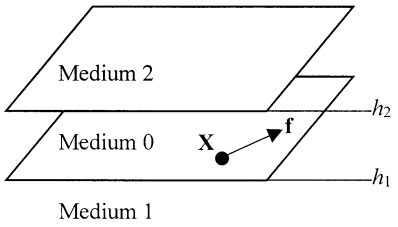

Fig. 2. A trimaterial system to be incorporated in the MLCs as shown in Fig. 1. The middle sandwiched layer (medium 0) represents the $m_{\mathbf{X}}$th layer which contains the source point, **X**. The lower half-space (medium 1) consists of the medium right below the $m_{\mathbf{X}}$th layer, and the upper half-space (medium 2) consists of the medium right above the $m_{\mathbf{X}}$th layer.

source point **X** resides, i.e. $m = m_{\mathbf{X}} - 1$, $m = m_{\mathbf{X}}$, or $m = m_{\mathbf{X}} + 1$, the special solution is taken to include the first few terms of the expansion solution of the corresponding trimaterial system consisting of the $m_{\mathbf{X}}$th layer and the adjacent lower and upper layers with the latter both extended to half spaces. Otherwise, the special solution is equal to zero. A particular merit of the trimaterial expansion solution is that every term in the expansion series can be reduced to a line integral over a finite interval, i.e. a substantial reduction from the original 2D integral over an infinite plane. Furthermore, the first-order term, which corresponds to the homogeneous full-space solution, can be evaluated analytically in an explicit form [6–8]. Since these leading terms in the triamterial expansion solution share the singular and most of the near-singular behaviors due to the source load and the image loads caused by the material mismatches among the total solution, the remaining general-part solution that requires a numerical 2D integration may be regularized substantially. In the following, for the sake of a complete description, the trimaterial expansion solution is introduced briefly while a detailed derivation can be found in Yang and Pan [9].

The trimaterial system is shown schematically in Fig. 2. While medium 0 represents the $m_{\mathbf{X}}$th layer where the source point **X** resides, media 1 and 2 represent the materials right below and right above the $m_{\mathbf{X}}$th layer, respectively. The media 1 and 2 both are extended to half spaces. If the $m_{\mathbf{X}}$th layer is the bottom or the top layer of the plate, the medium 1 or 2 then is taken to be empty, as a special case of the trimaterials. Furthermore, h_1 represents the vertical level of the $(m_{\mathbf{X}} - 1)$th interface, and h_2 the vertical level of the $m_{\mathbf{X}}$th interface.

The expansion solutions for the triamterials can be expressed in the form as

$$\tilde{\mathbf{r}}_0^*(x_3) = \mathrm{e}^{\mathrm{i}y_\alpha X_\alpha}\left[\tilde{\mathbf{r}}_0^{*(0)}(x_3) + \sum_{n=1}^{\infty}\tilde{\mathbf{r}}_0^{*(n)}(x_3)\right]$$

$$= \mathrm{e}^{\mathrm{i}y_\alpha X_\alpha}\left[\tilde{\mathbf{r}}_0^{*(0)}(x_3) + \sum_{n=1}^{\infty}\left(\tilde{\mathbf{r}}_{01}^{*(n)}(x_3) + \tilde{\mathbf{r}}_{02}^{*(n)}(x_3)\right)\right],$$

for $h_1 < x_3 < h_2$ (medium 0), (25)

$$\tilde{\mathbf{r}}_1^*(x_3) = \mathrm{e}^{\mathrm{i}y_\alpha X_\alpha}\left[\tilde{\mathbf{r}}_1^{*(0)}(x_3) + \sum_{n=1}^{\infty}\tilde{\mathbf{r}}_1^{*(n)}(x_3)\right], \tag{26}$$

for $x_3 < h_1$ (medium 1),

$$\tilde{\mathbf{r}}_2^*(x_3) = \mathrm{e}^{\mathrm{i}y_\alpha X_\alpha}\left[\tilde{\mathbf{r}}_2^{*(0)}(x_3) + \sum_{n=1}^{\infty}\tilde{\mathbf{r}}_2^{*(n)}(x_3)\right], \tag{27}$$

for $x_3 > h_2$ (medium 2),

where **r** represents **u**, **t**, **s** and their derivatives. The zero-order terms are the homogeneous full-space solutions for the medium where **x** resides and their Fourier inverse transform has been found analytically in an explicit form [6–8].

The zero-order terms (homogeneous full-space solutions) are given by

$$\tilde{\mathbf{u}}^{*(0)}(x_3) = \begin{cases} \mathrm{i}\eta^{-1}\mathbf{A}\langle \mathrm{e}^{-\mathrm{i}\mathbf{p}\eta(x_3 - X_3)}\rangle\mathbf{A}^{-1}(\mathbf{M} - \bar{\mathbf{M}})^{-1}, & x_3 < X_3 \\ \mathrm{i}\eta^{-1}\bar{\mathbf{A}}\langle \mathrm{e}^{-\mathrm{i}\bar{\mathbf{p}}\eta(x_3 - X_3)}\rangle\bar{\mathbf{A}}^{-1}(\mathbf{M} - \bar{\mathbf{M}})^{-1}, & x_3 > X_3 \end{cases}, \tag{28}$$

$$\tilde{\mathbf{t}}^{*(0)}(x_3) = \begin{cases} \mathbf{B}\langle \mathrm{e}^{-\mathrm{i}\mathbf{p}\eta(x_3 - X_3)}\rangle\mathbf{A}^{-1}(\mathbf{M} - \bar{\mathbf{M}})^{-1}, & x_3 < X_3 \\ \bar{\mathbf{B}}\langle \mathrm{e}^{-\mathrm{i}\bar{\mathbf{p}}\eta(x_3 - X_3)}\rangle\bar{\mathbf{A}}^{-1}(\mathbf{M} - \bar{\mathbf{M}})^{-1}, & x_3 > X_3 \end{cases}, \tag{29}$$

$$\tilde{\mathbf{s}}^{*(0)}(x_3) = \begin{cases} \mathbf{C}\langle \mathrm{e}^{-\mathrm{i}\mathbf{p}\eta(x_3 - X_3)}\rangle\mathbf{A}^{-1}(\mathbf{M} - \bar{\mathbf{M}})^{-1}, & x_3 < X_3 \\ \bar{\mathbf{C}}\langle \mathrm{e}^{-\mathrm{i}\bar{\mathbf{p}}\eta(x_3 - X_3)}\rangle\bar{\mathbf{A}}^{-1}(\mathbf{M} - \bar{\mathbf{M}})^{-1}, & x_3 > X_3 \end{cases}, \tag{30}$$

$$\tilde{\mathbf{u}}_{,X_\alpha}^{*(0)}(x_3) = \begin{cases} -y_\alpha\eta^{-1}\mathbf{A}\langle \mathrm{e}^{-\mathrm{i}\mathbf{p}\eta(x_3 - X_3)}\rangle\mathbf{A}^{-1}(\mathbf{M} - \bar{\mathbf{M}})^{-1}, & x_3 < X_3 \\ -y_\alpha\eta^{-1}\bar{\mathbf{A}}\langle \mathrm{e}^{-\mathrm{i}\bar{\mathbf{p}}\eta(x_3 - X_3)}\rangle\bar{\mathbf{A}}^{-1}(\mathbf{M} - \bar{\mathbf{M}})^{-1}, & x_3 > X_3 \end{cases}, \tag{31}$$

$$\tilde{\mathbf{t}}_{,X_\alpha}^{*(0)}(x_3) = \begin{cases} \mathrm{i}y_\alpha\mathbf{B}\langle \mathrm{e}^{-\mathrm{i}\mathbf{p}\eta(x_3 - X_3)}\rangle\mathbf{A}^{-1}(\mathbf{M} - \bar{\mathbf{M}})^{-1}, & x_3 < X_3 \\ \mathrm{i}y_\alpha\bar{\mathbf{B}}\langle \mathrm{e}^{-\mathrm{i}\bar{\mathbf{p}}\eta(x_3 - X_3)}\rangle\bar{\mathbf{A}}^{-1}(\mathbf{M} - \bar{\mathbf{M}})^{-1}, & x_3 > X_3 \end{cases}, \tag{32}$$

$$\tilde{\mathbf{s}}_{,X_\alpha}^{*(0)}(x_3) = \begin{cases} \mathrm{i}y_\alpha\mathbf{C}\langle \mathrm{e}^{-\mathrm{i}\mathbf{p}\eta(x_3 - X_3)}\rangle\mathbf{A}^{-1}(\mathbf{M} - \bar{\mathbf{M}})^{-1}, & x_3 < X_3 \\ \mathrm{i}y_\alpha\bar{\mathbf{C}}\langle \mathrm{e}^{-\mathrm{i}\bar{\mathbf{p}}\eta(x_3 - X_3)}\rangle\bar{\mathbf{A}}^{-1}(\mathbf{M} - \bar{\mathbf{M}})^{-1}, & x_3 > X_3 \end{cases}, \tag{33}$$

$$\tilde{\mathbf{u}}_{,X_3}^{*(0)}(x_3) = \begin{cases} -\mathbf{A}\langle\mathbf{p}\rangle\langle \mathrm{e}^{-\mathrm{i}\mathbf{p}\eta(x_3 - X_3)}\rangle\mathbf{A}^{-1}(\mathbf{M} - \bar{\mathbf{M}})^{-1}, & x_3 < X_3 \\ -\bar{\mathbf{A}}\langle\bar{\mathbf{p}}\rangle\langle \mathrm{e}^{-\mathrm{i}\bar{\mathbf{p}}\eta(x_3 - X_3)}\rangle\bar{\mathbf{A}}^{-1}(\mathbf{M} - \bar{\mathbf{M}})^{-1}, & x_3 > X_3 \end{cases}, \tag{34}$$

$$\tilde{\mathbf{t}}_{,X_3}^{*(0)}(x_3) = \begin{cases} \mathbf{B}\langle\mathrm{i}\mathbf{p}\eta\rangle\langle \mathrm{e}^{-\mathrm{i}\mathbf{p}\eta(x_3 - X_3)}\rangle\mathbf{A}^{-1}(\mathbf{M} - \bar{\mathbf{M}})^{-1}, & x_3 < X_3 \\ \bar{\mathbf{B}}\langle\mathrm{i}\bar{\mathbf{p}}\eta\rangle\langle \mathrm{e}^{-\mathrm{i}\bar{\mathbf{p}}\eta(x_3 - X_3)}\rangle\bar{\mathbf{A}}^{-1}(\mathbf{M} - \bar{\mathbf{M}})^{-1}, & x_3 > X_3 \end{cases}, \tag{35}$$

$$\tilde{\mathbf{s}}^{*(0)}_{X_3}(x_3)=\begin{cases}\mathbf{C}\langle \mathrm{i}\mathbf{p}\eta\rangle\langle \mathrm{e}^{-\mathrm{i}\mathbf{p}\eta(x_3-X_3)}\rangle\mathbf{A}^{-1}(\mathbf{M}-\bar{\mathbf{M}})^{-1}, & x_3<X_3\\ \bar{\mathbf{C}}\langle \mathrm{i}\bar{\mathbf{p}}\eta\rangle\langle \mathrm{e}^{-\mathrm{i}\bar{\mathbf{p}}\eta(x_3-X_3)}\rangle\bar{\mathbf{A}}^{-1}(\mathbf{M}-\bar{\mathbf{M}})^{-1}, & x_3>X_3\end{cases} \tag{36}$$

where $\mathrm{M}\equiv \mathrm{BA}^{-1}$. The above expressions are valid for $\mathbf{x}\in$ anyone of the three media with the matrices $\mathbf{A}$, $\mathbf{B}$ and $\mathbf{C}$ and vector $\mathbf{p}$ being associated to that medium.

The subsequent terms of displacement ($n\geq 1$) are given recursively by

$$\tilde{\mathbf{u}}^{*(1)}_{01}(x_3)=\bar{\mathbf{A}}_0\langle \mathrm{e}^{-\mathrm{i}\bar{\mathbf{p}}_0\eta(x_3-h_1)}\rangle\bar{\mathbf{A}}_0^{-1}(\mathbf{M}_1-\bar{\mathbf{M}}_0)^{-1}\times(\mathbf{M}_0-\mathbf{M}_1)\tilde{\mathbf{u}}^{*(0)}_0(h_1) \tag{37}$$

$$\tilde{\mathbf{u}}^{*(1)}_{02}(x_3)=\mathbf{A}_0\langle \mathrm{e}^{-\mathrm{i}\mathbf{p}_0\eta(x_3-h_2)}\rangle\mathbf{A}_0^{-1}(\bar{\mathbf{M}}_2-\mathbf{M}_0)^{-1}\times(\bar{\mathbf{M}}_2-\bar{\mathbf{M}}_0)\tilde{\mathbf{u}}^{*(0)}_0(h_2) \tag{38}$$

$$\tilde{\mathbf{u}}^{*(1)}_{1}(x_3)=-\tilde{\mathbf{u}}^{*(0)}_1(x_3)+\mathbf{A}_1\langle \mathrm{e}^{-\mathrm{i}\mathbf{p}_1\eta(x_3-h_1)}\rangle\mathbf{A}_1^{-1}(\mathbf{M}_1-\bar{\mathbf{M}}_0)^{-1}\times(\mathbf{M}_0-\bar{\mathbf{M}}_0)\tilde{\mathbf{u}}^{*(0)}_0(h_1) \tag{39}$$

$$\tilde{\mathbf{u}}^{*(1)}_{2}(x_3)=-\tilde{\mathbf{u}}^{*(0)}_2(x_3)+\bar{\mathbf{A}}_2\langle \mathrm{e}^{-\mathrm{i}\bar{\mathbf{p}}_2\eta(x_3-h_2)}\rangle\bar{\mathbf{A}}_2^{-1}(\bar{\mathbf{M}}_2-\mathbf{M}_0)^{-1}\times(\bar{\mathbf{M}}_0-\mathbf{M}_0)\tilde{\mathbf{u}}^{*(0)}_0(h_2) \tag{40}$$

for $n=1$, and

$$\tilde{\mathbf{u}}^{*(n)}_{01}(x_3)=\bar{\mathbf{A}}_0\langle \mathrm{e}^{-\mathrm{i}\bar{\mathbf{p}}_0\eta(x_3-h_1)}\rangle\bar{\mathbf{A}}_0^{-1}(\mathbf{M}_1-\bar{\mathbf{M}}_0)^{-1}\times(\mathbf{M}_0-\mathbf{M}_1)\tilde{\mathbf{u}}^{*(n-1)}_{02}(h_1) \tag{41}$$

$$\tilde{\mathbf{u}}^{*(n)}_{02}(x_3)=\mathbf{A}_0\langle \mathrm{e}^{-\mathrm{i}\mathbf{p}_0\eta(x_3-h_2)}\rangle\mathbf{A}_0^{-1}(\bar{\mathbf{M}}_2-\mathbf{M}_0)^{-1}\times(\bar{\mathbf{M}}_0-\bar{\mathbf{M}}_2)\tilde{\mathbf{u}}^{*(n-1)}_{01}(h_2) \tag{42}$$

$$\tilde{\mathbf{u}}^{*(n)}_{1}(x_3)=\mathbf{A}_1\langle \mathrm{e}^{-\mathrm{i}\mathbf{p}_1\eta(x_3-h_1)}\rangle\mathbf{A}_1^{-1}(\mathbf{M}_1-\bar{\mathbf{M}}_0)^{-1}\times(\mathbf{M}_0-\bar{\mathbf{M}}_0)\tilde{\mathbf{u}}^{*(n-1)}_{02}(h_1) \tag{43}$$

$$\tilde{\mathbf{u}}^{*(n)}_{2}(x_3)=\bar{\mathbf{A}}_2\langle \mathrm{e}^{-\mathrm{i}\bar{\mathbf{p}}_2\eta(x_3-h_2)}\rangle\bar{\mathbf{A}}_2^{-1}(\bar{\mathbf{M}}_2-\mathbf{M}_0)^{-1}\times(\bar{\mathbf{M}}_0-\mathbf{M}_0)\tilde{\mathbf{u}}^{*(n-1)}_{01}(h_2) \tag{44}$$

for $n=2,3,\ldots,\infty$. It is noted that the above solutions are valid only for $h_1<X_3<h_2$, while the general case, where the source point $\mathbf{X}$ resides in either medium of the tri-materials, has been discussed in detail by Yang and Pan [9].

The subsequent expansion terms for stresses ($n\geq 1$) are related to the same-order terms of displacement by

$$\tilde{\mathbf{t}}^{*(n)}_{01}(x_3)=-\mathrm{i}\eta\bar{\mathbf{M}}_0\tilde{\mathbf{u}}^{*(n)}_{01}(x_3),\qquad \tilde{\mathbf{s}}^{*(n)}_{01}(x_3)=-\mathrm{i}\eta\bar{\mathbf{N}}_0\tilde{\mathbf{u}}^{*(n)}_{01}(x_3) \tag{45}$$

$$\tilde{\mathbf{t}}^{*(n)}_{02}(x_3)=-\mathrm{i}\eta\mathbf{M}_0\tilde{\mathbf{u}}^{*(n)}_{02}(x_3),\qquad \tilde{\mathbf{s}}^{*(n)}_{02}(x_3)=-\mathrm{i}\eta\mathbf{N}_0\tilde{\mathbf{u}}^{*(n)}_{02}(x_3) \tag{46}$$

$$\tilde{\mathbf{t}}^{*(n)}_{1}(x_3)=-\mathrm{i}\eta\mathbf{M}_1\tilde{\mathbf{u}}^{*(n)}_{1}(x_3),\qquad \tilde{\mathbf{s}}^{*(n)}_{1}(x_3)=-\mathrm{i}\eta\mathbf{N}_1\tilde{\mathbf{u}}^{*(n)}_{1}(x_3) \tag{47}$$

$$\tilde{\mathbf{t}}^{*(n)}_{2}(x_3)=-\mathrm{i}\eta\bar{\mathbf{M}}_2\tilde{\mathbf{u}}^{*(n)}_{2}(x_3),\qquad \tilde{\mathbf{s}}^{*(n)}_{2}(x_3)=-\mathrm{i}\eta\bar{\mathbf{N}}_2\tilde{\mathbf{u}}^{*(n)}_{2}(x_3) \tag{48}$$

where $\mathbf{M}$ is defined earleir and $\mathbf{N}\equiv\mathbf{CA}^{-1}$.

The expansion terms for the derivatives of displacement and stress with respect to source coordinates have the same expressions as in Eqs. (37)–(44) provided that the notations for the displacement and the stress are replaced by those for their derivatives correspondingly. For brevity, these expressions are not documented in the text.

The above expansion solutions in the transform domain may be inverted to their counterparts in the physical domain by applying the inverse transform operator (23) or (24). However, the expansion solutions possess certain unique features that allow an analytical reduction of the integral dimensions in the Fourier inverse transforms, as described below.

To reduce the integral dimensions, an explicit expression for the transform-domain expansion solution first is developed, term-by-term, on the base of the homogeneous full-space solution. Without loss of generality, it is found that the expansion terms for the displacement can be written as

$$\tilde{\mathbf{u}}^{*(N)}=\eta^{-1}\mathbf{J}_{N+1}\langle \mathrm{e}^{-\mathrm{i}\boldsymbol{\beta}_N\eta}\rangle\mathbf{J}_N\cdots\langle \mathrm{e}^{-\mathrm{i}\boldsymbol{\beta}_n\eta}\rangle\mathbf{J}_n\cdots\langle \mathrm{e}^{-\mathrm{i}\boldsymbol{\beta}_0\eta}\rangle\mathbf{J}_0 \tag{49}$$

where the tensors $\mathbf{J}_n$ and vectors $\boldsymbol{\beta}_n$ are functions of θ but are independent of η. It can be shown that the above notational expression times η holds for the in-plane stress tensor $\mathbf{s}^*$, traction tensor $\mathbf{t}^*$ and derivatives of $\mathbf{u}^*$, and further times η holds for the derivatives of $\mathbf{s}^*$ and $\mathbf{t}^*$.

Inserting these expressions multiplied by $\mathrm{e}^{\mathrm{i}y_\alpha X_\alpha}$ to the inverse transform operator (24) gives

$$\begin{aligned}\mathbf{u}^{*(N)}&=\frac{1}{(2\pi)^2}\int\!\!\int\eta\tilde{\mathbf{u}}^{*(N)}\,\mathrm{e}^{\mathrm{i}y_\alpha(X_\alpha-x_\alpha)}\,\mathrm{d}\eta\,\mathrm{d}\theta\\&=\frac{1}{(2\pi)^2}\int\!\!\int\mathbf{J}_{N+1}\langle \mathrm{e}^{-\mathrm{i}\boldsymbol{\beta}_N\eta}\rangle\mathbf{J}_N\cdots\langle \mathrm{e}^{-\mathrm{i}\boldsymbol{\beta}_n\eta}\rangle\mathbf{J}_n\cdots\langle \mathrm{e}^{-\mathrm{i}\boldsymbol{\beta}_0\eta}\rangle\\&\quad\times\mathbf{J}_0\,\mathrm{e}^{\mathrm{i}y_\alpha(X_\alpha-x_\alpha)}\,\mathrm{d}\eta\,\mathrm{d}\theta\end{aligned} \tag{50}$$

for the displacement $\mathbf{u}^*$, and

$$\begin{aligned}>\mathbf{t}^{*(N)}&=\frac{1}{(2\pi)^2}\int\!\!\int\tilde{\mathbf{t}}^{*(N)}\,\mathrm{e}^{\mathrm{i}y_\alpha(X_\alpha-x_\alpha)}\,\mathrm{d}\eta\,\mathrm{d}\theta\\&=\frac{1}{(2\pi)^2}\int\!\!\int\eta\mathbf{J}_{N+1}\langle \mathrm{e}^{-\mathrm{i}\boldsymbol{\beta}_N\eta}\rangle\mathbf{J}_N\cdots\langle \mathrm{e}^{-\mathrm{i}\boldsymbol{\beta}_n\eta}\rangle\mathbf{J}_n\cdots\langle \mathrm{e}^{-\mathrm{i}\boldsymbol{\beta}_0\eta}\rangle\\&\quad\times\mathbf{J}_0\,\mathrm{e}^{\mathrm{i}y_\alpha(X_\alpha-x_\alpha)}\,\mathrm{d}\eta\,\mathrm{d}\theta\end{aligned} \tag{51}$$

for the traction $\mathbf{t}^*$. Whilst the same expression as in Eq. (51) holds for the in-plane stress $\mathbf{s}^*$ and the derivative of displacement $\mathbf{u}^*_{,X_k}$, the derivative of the traction tensor $\mathbf{t}^*$ is

found to be

$$\mathbf{t}^{*(N)}_{,X_k} = \frac{1}{(2\pi)^2}\int\int \eta \tilde{\mathbf{t}}^{*(N)}_{,X_k}\, \mathrm{e}^{\mathrm{i}y_\alpha(X_\alpha - x_\alpha)}\,\mathrm{d}\eta\,\mathrm{d}\theta$$
$$= \frac{1}{(2\pi)^2}\int\int \eta^2 \mathbf{J}_{N+1}\langle \mathrm{e}^{-\mathrm{i}\boldsymbol{\beta}_N\eta}\rangle \mathbf{J}_N \cdots \langle \mathrm{e}^{-\mathrm{i}\boldsymbol{\beta}_n\eta}\rangle \mathbf{J}_n \cdots \langle \mathrm{e}^{-\mathrm{i}\boldsymbol{\beta}_0\eta}\rangle$$
$$\times \mathbf{J}_0\, \mathrm{e}^{\mathrm{i}y_\alpha(X_\alpha - x_\alpha)}\,\mathrm{d}\eta\,\mathrm{d}\theta \tag{52}$$

with the same expression for the derivative of $\mathbf{s}^*$.

Now, by writing the above integrants in index form, it can be seen that the 2D integrals in Eqs. (50)–(52) are reducible to a line integral by carrying out the integral in η over $(0,\infty)$. The reduced integrals are given by

$$u^{*(N)}_{ji} = \frac{1}{(2\pi)^2}\oint_{2\pi} G_{ji}\left(\frac{1}{s} + \mathrm{i}\delta(s)\right)\mathrm{d}\theta, \tag{53}$$

$$t^{*(N)}_{ji} = \frac{1}{(2\pi)^2}\oint_{2\pi} G_{ji}\left(-\frac{1}{s^2} + \mathrm{i}\delta'(s)\right)\mathrm{d}\theta, \tag{54}$$

$$t^{*(N)}_{ji,X_k} = \frac{1}{(2\pi)^2}\oint_{2\pi} G_{ji}\left(-\frac{2}{s^3} - \mathrm{i}\delta''(s)\right)\mathrm{d}\theta, \tag{55}$$

where $\delta(s)$ is the Dirac delta, the primes indicate the order of derivatives, and

$$G_{ji} = (J_{jk_{N+1}})_{N+1}(J_{k_{N+1}k_N})_N \cdots (J_{k_{n+1}k_n})_n \cdots (J_{k_1 i})_0, \tag{56}$$

$$s = (\beta_{k_{N+1}})_N + \cdots (\beta_{k_{n+1}})_n + \cdots (\beta_{k_1})_0 - ((X_1 - x_1)\cos\theta + (X_2 - x_2)\sin\theta). \tag{57}$$

Note that while the expression (54) holds valid also for $\mathbf{s}^*$ and $\mathbf{u}^*_{,X_k}$, the expression (55) also for $\mathbf{s}^*_{,X_k}$. However, all these functions have their own G_{ji} and s, different from one another in general. Furthermore, it is observed that Eqs. (53)–(55) become finite-part integrals when $s = 0$, occurring in the first-order term ($N = 1$) when the source and field points are on the same interface plane. This is similar to the bimaterial situation where the source and field points are both on the interface, as has been mentioned by Pan and Yuan [4].

4. Numerical implementation

In this section, the newly proposed numerical approach for the evaluation of the 3D anisotropic elastostatic Green's functions in MLCs is implemented. As mentioned before, if the field point $\mathbf{x}$ is located in a layer adjacent to or the same as layer $m_\mathbf{X}$ where the source point $\mathbf{X}$ resides, i.e. $m = m_\mathrm{X} - 1$, $m = m_\mathrm{X}$, or $m = m_\mathrm{X} + 1$, the special solution is taken to include the first few terms of the expansion solution of the corresponding full-space trimaterial system consisting of the $m_\mathbf{X}$th layer medium and the adjacent lower and upper media. Otherwise, it is equal to zero. This novel scheme is written as

$$\tilde{\mathbf{r}}^{*(s)}(x_3) = \sum_{n=0}^{N} \tilde{\mathbf{r}}^{*(n)}(x_3), \quad \text{for } m = m_\mathrm{X} - 1,\ m = m_\mathrm{X},$$
$$\text{or } m = m_\mathrm{X} + 1, \tag{58}$$

where $\mathbf{r}$ represents $\mathbf{u}$, $\mathbf{t}$, $\mathbf{s}$ and their derivatives, N is a finite integer, and $\tilde{\mathbf{r}}^{*(n)}$ represents the nth term in the trimaterial expansion solution as described in the Section 3. Otherwise,

$$\tilde{\mathbf{r}}^{*(s)}(x_3) = 0. \tag{59}$$

Therefore, by inserting these special solutions into Eqs. (18)–(21) for $\mathbf{V}_m$ and $\mathbf{W}_m$ and similar equations for $\mathbf{V}'_m$ and $\mathbf{W}'_m$, the general part of the Green's functions can be obtained in the transform domain by solving these equations. Then, the general part is transformed back to the physical counterpart by a numerical 2D integration over the infinite plane while the special solution, except for the zero-order term which is inverted analytically in an explicit form [6–8], is inverted by a line integration over a finite interval. In the following, the Green's functions in a plate made of five orthortropic layers are examined to show the efficiency of the proposed approach. Furthermore, the characteristics of the Green's functions are analyzed in both the transform and the physical domains.

The plate examined is made of five equal-thickness layers ($h_0 = 0$, $h_1 = 0.2$, $h_2 = 0.4$, $h_3 = 0.6$, $h_4 = 0.8$, $h_5 = 1$) of the same orthortropic material but each in a different angle of in-plane rotation. More specifically, the stacking sequence of the layers is (0/45/−45/30/−30°) from the bottom to top. The normalized materials constants of the 0°-layer are: the Young's moduli $E_1 = 1$, $E_2 = E_3 = 0.1$, the shear moduli $\mu_{13} = \mu_{23} = \mu_{12} = 1/30$, and the Poisson's ratios $\nu_{12} = \nu_{23} = \nu_{13} = 0.336$. To carry out the numerical line integral and 2D integral, an adaptive quadrature scheme, developed previously by the authors [16], is used. The adaptive mesh is generated nonuniformly based on the local deviation of the Green's function variation from a quadrature interpolation subject to a critical convergence control. In the 2D case, the integral is carried out using Eq. (24) in the polar coordinates. In the following calculations, the source point is fixed at (0,0,0.5), in the middle plane of the composite plate.

First, the characteristics of the elastic fields due to the point force in the plate are examined. Under the configuration described above, the Green's functions including displacement, stress, and their derivatives are evaluated along a vertical line at $(0.5,0,x_3)$ through the plate thickness. One hundred equally-spaced points are selected along the line. The evaluation was carried out with N taken to be 1 in Eq. (58), i.e. by inserting the zero- and first-order terms in the special solution. The variations of some of the Green's function components are plotted in Figs. 3–5: Fig. 3 shows the Green's displacement and stress due to the point force acting in the X_1- and X_3-axes; Fig. 4 shows their derivatives

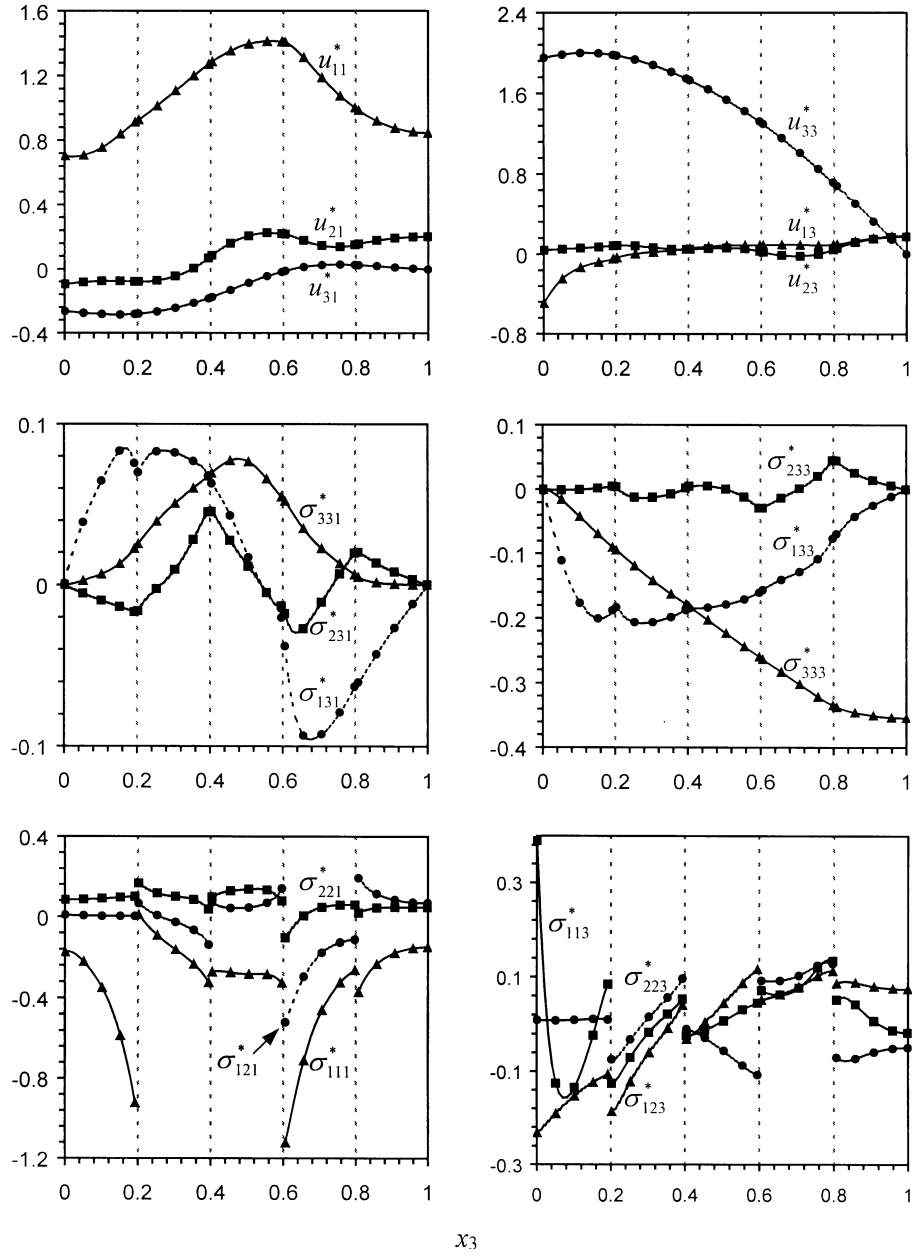

Fig. 3. Variation of the Green's displacement and stress components along a vertical line (0.5,0,x_3) in a composite plate consisting of five identical orthortropic plies in stacking sequence (0/45/−45/30/−30°) from the bottom to top. The source point is located at (0,0,0.5) in the middle plane of the composite plate.

with respect to X_1; and Fig. 5 shows their derivatives with respect to X_3. From these figures, it can be seen that these solutions clearly satisfy the boundary and interfacial conditions, Eqs. (4)–(6). Also, it is seen that the displacement variations in the vertical direction are smooth due to the weak material mismatch in this direction. However, the out-of-plane stress components (i.e. the traction **t**-vector), though continuous, are kinked at the interfaces. Meanwhile, the in-plane stress components (i.e. the in-plane **s**-vector) are discontinuous across the interfaces, expectedly, due to the strong materials mismatch in the in-plane directions caused by the ply-rotations.

The same problem then is solved by taking $N = 0$ (zero-term) and 2 (zero-, first-, and second-terms) in Eq. (58). The solutions are compared with the previous one ($N = 1$). It is found that the relative differences among the three sets of solution are within 10^{-5}. This small difference, compared with the dominant component magnitude at about 10^0, suggests the validity of the developed theory and numerical programming. However, the CPU time needed to complete the 2D integration of the general-part solution with $N = 0$ was about eight times of that with $N = 1$, under the same convergence control and condition of computer power. The corresponding CPU times for $N = 2$ and $N = 1$, on the other hand, were nearly the same. Since the computation of the general-part solution involves the solution of the system of

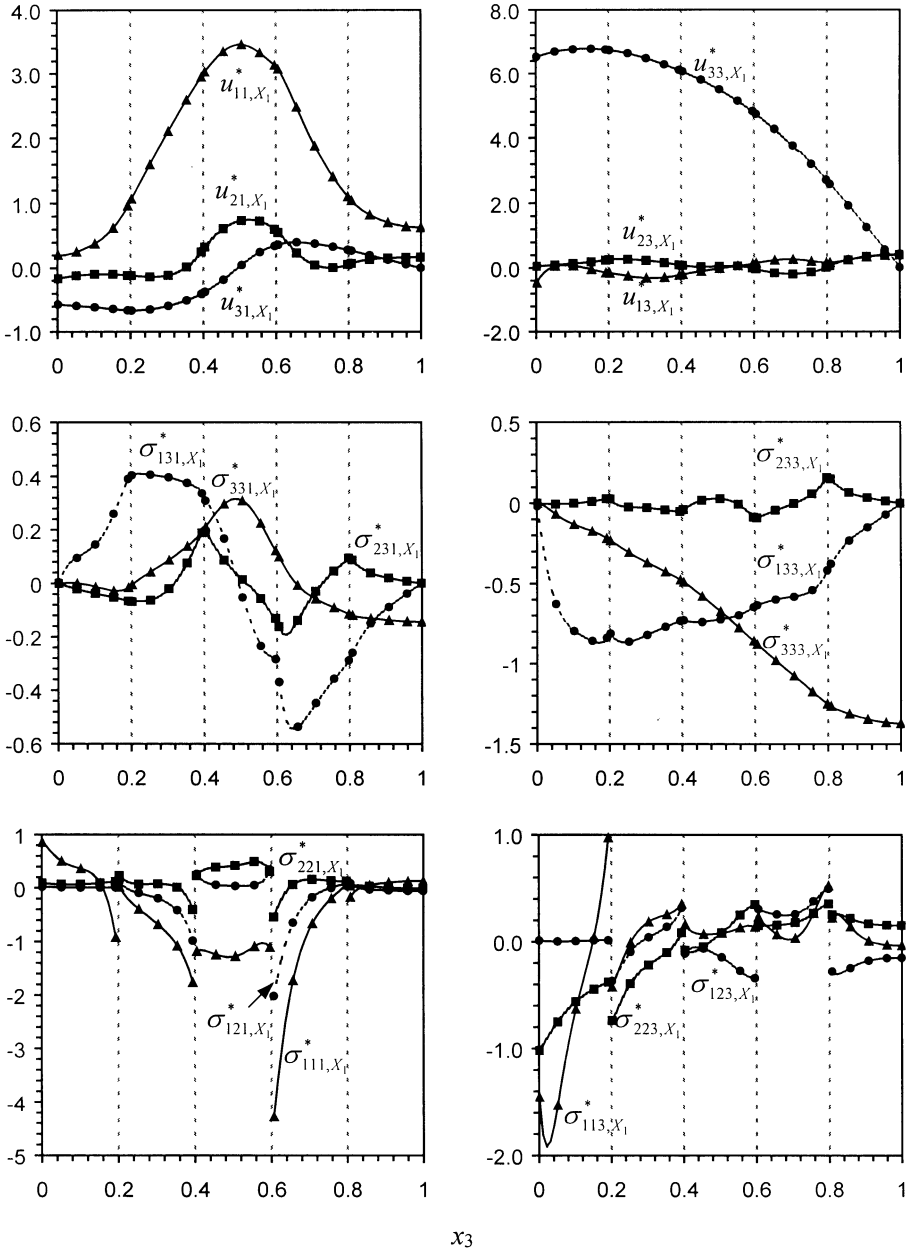

Fig. 4. Variation of the derivatives of the Green's displacement and stress components with respect to X_1 along a vertical line (0.5,0,x_3) in a composite plate consisting of five identical orthortropic plies in stacking sequence (0/45/−45/30/−30°) from the bottom to top. The source point is located at (0,0,0.5) in the middle plane of the composite plate.

Eqs. (18)–(21) for $\mathbf{V}_m$ and $\mathbf{W}_m$ (similarly for $\mathbf{V}'_m$ and $\mathbf{W}'_m$) as well as the numerical integration in the radial polar coordinate η, the computation effort in the special solution where these operations can be eliminated is negligible relatively. Therefore, while taking higher-order terms of the expansion solution shows no further reduction on the total computational effort, the incorporation of the zero- and first-order terms is considered to be optimal in regard to the efficiency of evaluation for the physical Green's functions in the material.

The reason for the significant improvement in the computational efficiency by the incorporation of the zero- and first-order terms, instead of the zero-order term, of the trimaterial expansion solution into the special solution is visualized in Figs. 6 and 7. The two figures show the transform-domain profiles for the general part of the Green's function components, $\tilde{u}^*_{33}$, $\tilde{\sigma}^*_{333}$, $\tilde{u}^*_{33,X_3}$, and $\tilde{\sigma}^*_{333,X_3}$, after the deduction of the zero-order term, and after the deduction of the zero- and first-order terms, respectively. The field point is located at (0.5,0,0.7) while other parameters are the same as in the previous calculations. It is obviously seen that the transform-domain general-part profiles of these representative Green's function components with $N = 1$ (Fig. 7) are more regular than those with $N = 0$

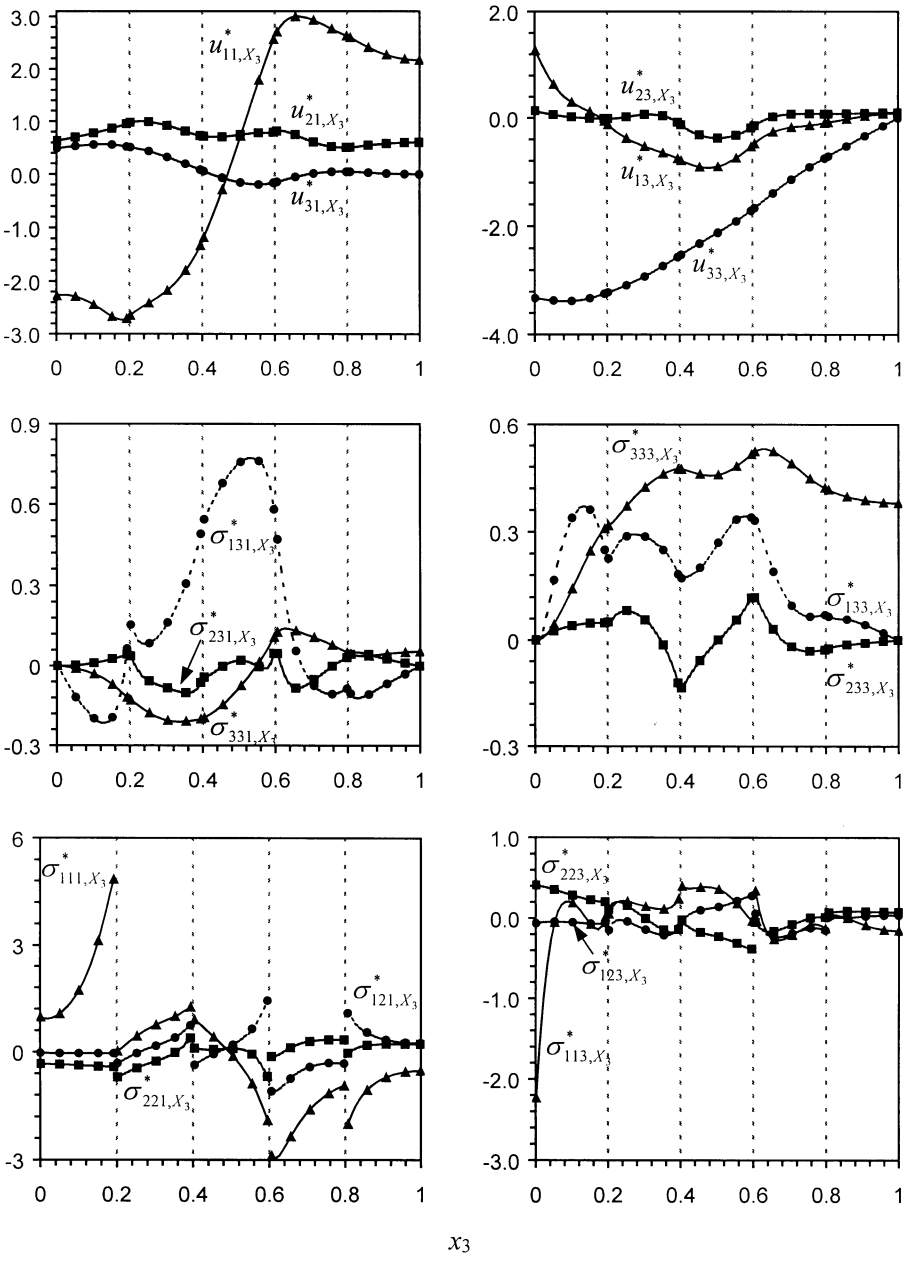

Fig. 5. Variation of the derivatives of the Green's displacement and stress components with respect to X_3 along a vertical line (0.5,0,x_3) in a composite plate consisting of five identical orthortropic plies in stacking sequence (0/45/−45/30/−30°) from the bottom to top. The source point is located at (0,0,0.5) in the middle plane of the composite plate.

(Fig. 6), in terms of the numbers of ridges and the size of the region that requires a highly resolved mesh. Note that the meshes shown in Figs. 6 and 7 are not the mesh used in the calculations. Furthermore, based on Figs. 6 and 7 and the adaptive mesh density used in the previous calculations, we have found that the FFT technique, although commonly used in many scientific and engineering applications, is not suitable to the present application. Since in the common FFT application, the mesh needs to be uniform, the FFT mesh of uniform density should be determined by the highest local mesh density as needed in the adaptive scheme for the same numerical accuracy, i.e. a bottle-neck effect. In our calculation using the adaptive scheme, the smallest spacing in terms of y_1 and y_2 was on the order of 10^{-4}. Considering the size of the region that should be covered, for instance over a 100×100 square as shown in Figs. 6 and 7, an application of the FFT technique to the present case simply appears to be unachievable with the contemporary computational power.

Finally, it should be mentioned that in the present B.V. problem formulated in Eqs. (3)–(7) under the conditions of traction-free bottom surface and rigid-smooth contact top surface, the transform-domain Green's displacement components, $\tilde{u}^*_{11}$, $\tilde{u}^*_{12}$, $\tilde{u}^*_{21}$ and $\tilde{u}^*_{22}$, are singular in terms of

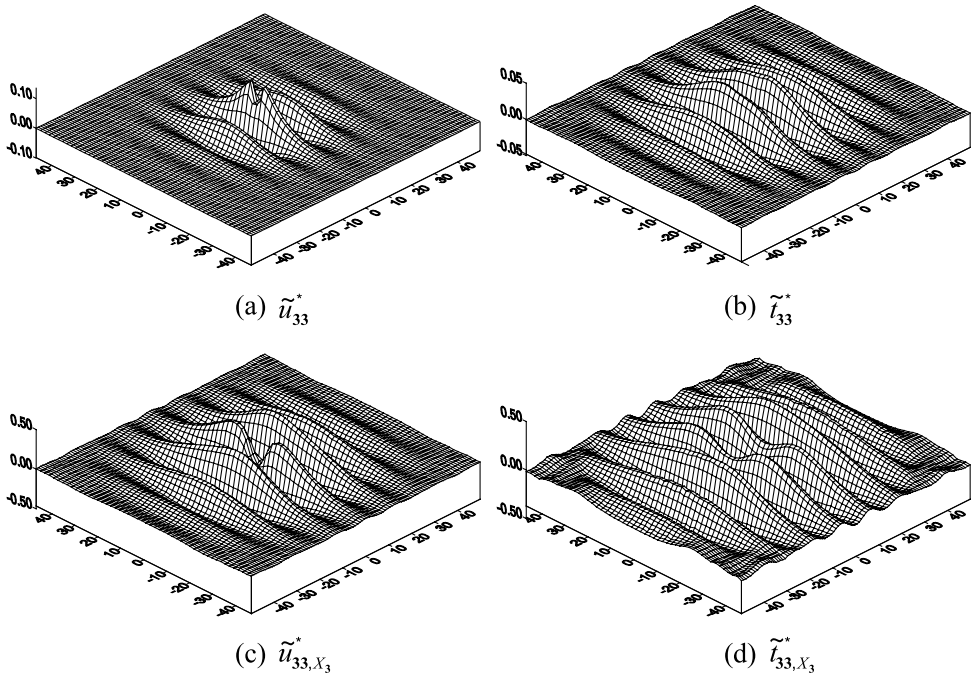

Fig. 6. Profiles of the general part of the Green's function components after deduction of the homogeneous full-space solution (zero-order term in the trimaterial expansion solution) in the Fourier transform domain (y_1,y_2): (a) $\tilde{u}^*_{33}$; (b) $\tilde{t}^*_{33}$; (c) $\tilde{u}^*_{33,X_3}$ and (d) $\tilde{t}^*_{33,X_3}$, with $X = (0, 0, 0.5)$ and $x = (0.5, 0, 0.7)$, in the composite plate.

η, on the first order of η^{-1}, at $\eta = 0$. The results described above are the ones after the subtraction of this singularity (with the amplitude numerically calibrated) from the original expressions. A detailed discussion on the validity and meaning of the singularity subtraction and other related singularities for 3D anisotropic plates under various boundary conditions has been given by Yang and Pan [18].

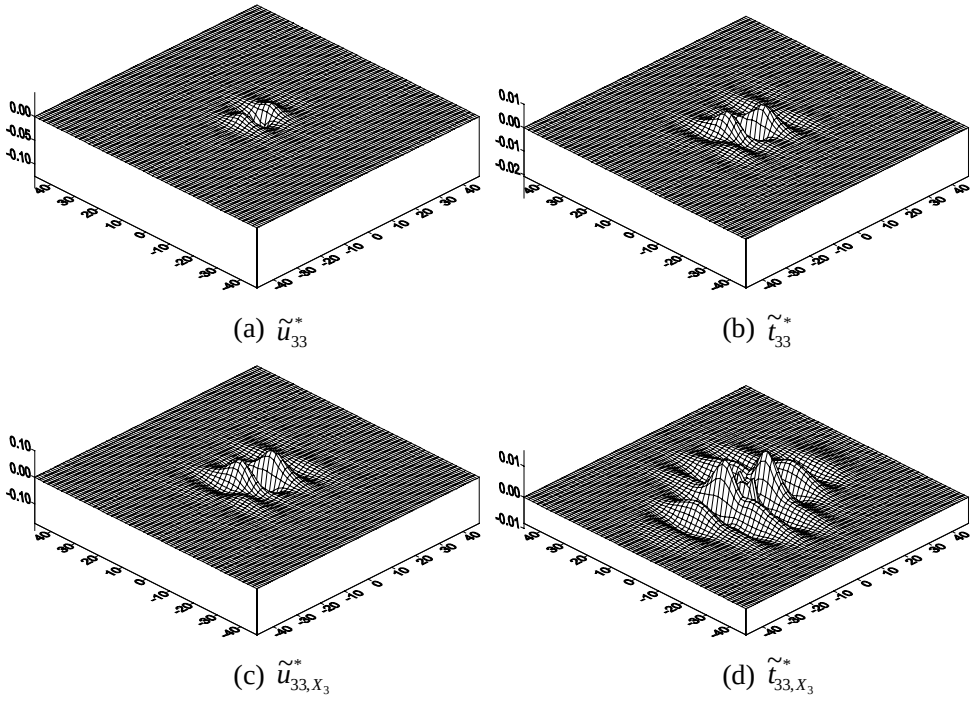

Fig. 7. Profiles of the general part of the Green's function components after deduction of the zero- and first-order terms of the trimaterial expansion solution in the Fourier transform domain (y_1,y_2): (a) $\tilde{u}^*_{33}$; (b) $\tilde{t}^*_{33}$; (c) $\tilde{u}^*_{33,X_3}$ and (d) $\tilde{t}^*_{33,X_3}$. The other conditions are the same as in Fig. 6.

5. Conclusions

Three-dimensional Green's functions, including displacement, stress and their derivatives, have been derived for anisotropic elastostatic MLCs for the first time using the Fourier transform method, the generalized Stroh formalism, and a novel superposition approach. These Green's functions are valid under the conditions of free traction on one surface and rigid-smooth contact on the other surface of the laminate plate, with welded conditions along the interfaces. The present formulation and solution procedure may easily be extended to other cases under different boundary and interfacial conditions. These Green's functions are essential to the BIE formulation for 3D anisotropic composite laminate problems with regular and cracked geometries. They can also be applied to solve 3D inclusion problems in modern physics, for example, the quantum dots problem in the special case of a half space [19].

The Green's functions of the MLCs are expressed in two parts, a general-part solution and a special solution. In the solution procedure, the special solution is given, and the general part is numerically solved under the boundary and interfacial conditions. Since the evaluation of the general-part solution involves inevitably a numerical 2D integration in an infinite plane and a solution of a large system of algebraic equations at each mesh point in the inverse transform, what a special solution is selected determines the efficiency of the evaluation for the Green's functions. We have proposed a novel approach to derive the special solution by incorporating the first few terms of the trimaterial expansion solution, recently developed by the authors [9]. The merit of the inserted trimaterial expansion solution is that every term in the expansion series can be reduced to a line integral over a finite interval, with the zero-order term corresponding to the homogeneous full-space solution previously derived in an explicit form [6–8]. Furthermore, the leading terms share the singular and most of the near-singular behaviors due to the source load and the image loads caused by the material mismatches. Therefore, in doing so, the remaining general-part solution that requires a numerical 2D integral evaluation becomes regular and the Green's functions overall can be evaluated efficiently.

For example, a five-layered orthortropic plate then is examined to demonstrate the validity of the theoretical development and efficiency of the proposed approach. It is found that the incorporation of the zero- and first-order terms of the trimaterial expansion solution produces the optimal efficiency of evaluation for the Green's functions. The detailed characteristics of the Green's functions in both the transform and the physical domains are also examined, indicating clearly the unsuitability of the uniform FFT technique in application to the present case.

Acknowledgements

The authors would like to thank Prof. F.G. Yuan of North Carolina State University for his encouragement and discussion. This project is supported in part by the AFOSR under Grant No. F33615-97-C-5089. Dr Richard Hall is the project manager.

References

[1] Mura T. Micromechanics of defects in solids. 2nd ed. Dordrecht: Martinus Nijhoff, 1987.
[2] Ting TCT. Anisotropic elasticity. Oxford: Oxford University Press, 1996.
[3] Wu KC. Generalization of the Stroh formalism to three-dimensional anisotropic elasticity. J Elasticity 1998;51:213–25.
[4] Pan E, Yuan FG. Three-dimensional Green's functions in anisotropic bimaterials. Int J Solids Struct 2000;37:5329–51.
[5] Barnett DM, Lothe J. Line force loadings on anisotropic half-spaces and wedges. Physica Norvegica 1975;8:13–22.
[6] Ting TCT, Lee VG. The three-dimensional elastostatic Green's function for general anisotropic linear elastic solids. Quart J Mech Appl Math 1997;50:407–26.
[7] Sales MA, Gray LJ. Evaluation of the anisotropic Green's functiton and its derivatives. Computers Struct 1998;69:247–54.
[8] Tonon F, Pan E, Amadei B. Green's functions and boundary element formulation for 3D anisotropic media. Computers Struct 2001;79:469–82.
[9] Yang B, Pan E. Three-dimensional Green's functions in anisotropic trimaterials. Int. J. Solids. Struct 2002 (in press).
[10] Fares N, Li VC. General image method in a plane-layered elastostatic medium. ASME J Appl Mech 1988;55:781–5.
[11] Yu HY, Sanday SC. Elastic fields due to centers of dilatation and thermal inhomogeneities in plane-layered solids. J Mech Phys Solids 1993;41:267–96.
[12] Shou KJ. A superposition scheme to obtain fundamental boundary element solutions in multi-layered elastic media. Int J Numer Analyt Methods Geomech 2000;24:795–814.
[13] Pan E. Static Green's functions in multilayered half spaces. Appl Mathl Modelling 1997;21:509–21.
[14] VelSenthil S, Batra RC. Generalized plane strain thermoelastic deformation of laminated anisotropic thick plates. Int J Solids Struct 2001;38:1395–414.
[15] Yuan FG, Yang S. Three-dimensional Green's functions for composite laminates and composite half-space. Submitted for publication, 2001.
[16] Pan E, Yang B, Cai G, Yuan FG. Stress analyses around holes in composite laminates using boundary element method. Engng Analysis Boundary Element 2001;35:31–40.
[17] Yang B. Examination of free-edge crack nucleation around an open hole in composite laminates. Submitted for publication, 2001.
[18] Yang B, Pan E. Three-dimensional Green's functions for anisotropic elastostatic multilayered plate under various boundary conditions. Submitted for publication, 2001.
[19] Pan E, Yang B. Elastostatic fields in an anisotropic substrate with a buried quantum dot. J Appl Phys 2001 90:6190–6.